

# We are IntechOpen, the world's leading publisher of Open Access books Built by scientists, for scientists

6,900

Open access books available

186,000

International authors and editors

200M

Downloads

Our authors are among the

154

Countries delivered to

TOP 1%

most cited scientists

12.2%

Contributors from top 500 universities



WEB OF SCIENCE™

Selection of our books indexed in the Book Citation Index  
in Web of Science™ Core Collection (BKCI)

Interested in publishing with us?  
Contact [book.department@intechopen.com](mailto:book.department@intechopen.com)

Numbers displayed above are based on latest data collected.  
For more information visit [www.intechopen.com](http://www.intechopen.com)



# Innovative Hybrid Materials with Improved Tensile Strength Obtained by 3D Printing

*Roxana Mioara Piticescu, Laura Madalina Cursaru, Gabriela Negroiu, Cristina Florentina Ciobota, Ciprian Neagoe and Daniel Safranchik*

## Abstract

Barium titanate (BT) and barium strontium titanate (BST) are one of the most studied ferroelectric materials with excellent piezoelectric properties, which can be used to stimulate bone formation by applying an electrical field. It is known that this ceramic is biocompatible and can be used for medical applications. New hybrid materials based on BT and collagen and BST and collagen, with potential applications in bone reconstruction, are presented, emphasizing the potential of fabricating 3D structures by integrating hydrothermal synthesis with additive manufacturing. Designing such structures may take advantage of rheological characterization at single-molecule level for some elastic biopolymers like titin and collagen and their molecular dissection into structural motifs that independently contribute to the protein viscoelasticity. Atomic force spectroscopy measurements on synthetic polypeptides showed that a polypeptide chain containing Ig domain modules is protected against rupture at high stretch by Ig domain unfolding, an important mechanism for stress relaxation in titin molecules. This property may be exploited to enhance the tensile strength of a 3D structure by adding specific synthetic polypeptides to the composition of the printing paste.

**Keywords:** barium titanate, barium strontium titanate, 3D printing, titin, Ig domain, fracture mechanics

## 1. Introduction

Bone defects occur due to malformations, traumatic lesions, and tumor resections. Biomaterials for bone defect reconstruction consist of osteosynthetic materials that are placed in the cavity left behind by osteotomies or traumatic lesions. Other applications refer to dental implants with functional or aesthetic role in the facial region. The results of bone reconstruction are dependent on the surgical skills, the quality of the adjacent tissue, the size and location of the bone defect, as well as the method of repairing the bone defect. Current methods of reconstruction include simple or vascularized bone grafts, the use of biomaterials, and, more recently, the use of growth factors to induce osteoinduction [1].

The use of autologous bone for orthopedic reconstruction may be restricted due to the limited amount of donor bone from the sampling areas. It is possible that the bone tissue taken may require reshaping into custom shapes, which may complicate the surgical operation. Also, complications in the case of simple bone grafts include graft resorption and increased mortality associated with the sampling area [1].

The benefits of alloplastic materials have been reported in the literature, being used as such or in combination with bone transplants or osteoinductive cytokines. The procedure can be used not only to replace the missing bone but also to stimulate osteoinduction, acting as a scaffold material for bone regeneration. The implanted materials should be biocompatible, without any side effects or toxicity. However, over time complications and toxicities of implanted biomaterials used in orthopedic surgery have been reported, often leading to inflammation associated with leukocytosis and fibrosis.

For osteosynthesis, titanium alloy prostheses offer major advantages in terms of biocompatibility, stability, and individual implant placement. Removal of asymptomatic prostheses and screws after fracture healing is still controversial due to the fact that the removal procedure could damage the bone [1].

The large variety of biomaterials for bone defect reconstruction makes it difficult to choose the right material for surgical areas and specific applications. An optimal biomaterial meets all the requirements: biocompatibility, stability, intra-operative matching, product safety, and low costs; in reality, the perfect material has not yet been found. The development of future materials aims to improve the physical and biological properties, especially regarding surface interactions [1].

While the popularity of hydroxyapatite-based ceramic materials as filler for critical bone defects is known in the community of specialists in bioengineering, materials science, and orthopedic and dental surgery, only a few studies address piezoelectric materials for bone regeneration, such as barium titanate (BT) [BaTiO<sub>3</sub>] and barium strontium titanate (BST) [Ba<sub>0.7</sub>Sr<sub>0.3</sub>TiO<sub>3</sub>]. The potential effect of this class of materials in bone tissue engineering is due to its dielectric properties, low dielectric loss, and polarization. Sr<sup>2+</sup> ion can increase a dielectric constant, and it is a trace element in the human body that plays a dual role in bone formation and regeneration [2].

On the other hand, barium titanate-based ceramic with perovskite structure has been widely used as a ferroelectric material for its attractive properties, such as high piezoelectric coefficient ( $d_{33} = 191$  pC/N) as well as excellent biocompatibility and bone regeneration capacity in the complex physiological environment, and is further considered as an intelligent material for tissue reconstruction [2–4].

Since 1954, it has been reported that natural bone is a piezoelectric material [5–12]. In 1957, Fukada et al. [8] observed that the stress-induced piezoelectric effect in bone was due to the slipping of collagen fibers past one another. The bone tissue exhibited a very low piezoelectric coefficient of 0.7 pC/N [13] and was demonstrated to be biologically active and would respond to micromechanical stress such as the movement of the body itself, leading to the generation of an electrical dipole [14, 15]. Piezoelectric materials can provide the electrical stimulation characteristic for natural bone environment as it has been asserted that bone growth and repair are promoted by the electrical signals produced when the bone is mechanically stressed [16]. Due to their parallel features with the real bone, piezoelectric materials for bone tissue reconstruction may become the next generation of bone grafts [17]. Piezoelectric property of barium titanate could be used as a charge supply to stimulate the bone implant healing process. So far, all the piezoelectric ceramics used in vivo and vitro were in the dense bulk form [18]. However, owing to the interconnected pores to provide a favorable environment for bone ingrowth and osseointegration [19], a functional bone implant should be porous [15], to

create strong bonds with the host natural tissue by allowing cellular penetration and encouraging new cells for tissue regeneration.

One of the best ways to achieve this goal is to use an osteoconductive and porous structure to act as a three-dimensional (3D) porous scaffold [2]. Ideally, osseointegration of the grafted material would be accomplished on a long timescale by the progressive action of osteoclasts, osteoblasts, and osteocytes which remove the graft material and deposit new bone in place [20]. Having a structure that resembles the natural design and composition may not always respond to functional requirements of a medical application. Bioresorbable scaffolds to replace bone defects must have a high porosity—a pore size of 50–800  $\mu\text{m}$ —to allow the infiltration of cells and nutrients into the implant [21]; the porosity of the material should accommodate new osteon growth, requiring 200  $\mu\text{m}$  pore size, to allow growth of new capillaries, optimal for 50  $\mu\text{m}$  pore size, whereas interconnected micropores lower than 10  $\mu\text{m}$  improve the metabolic environment and fluid circulation through capillarity [22]. The apparent conflicting requirements are met with a 3D design that does not correspond to the natural structure of the bone. Furthermore, improving the osmotic or mechanical properties of the synthetic bone graft material by adding components that are not present in the natural bone may address the needs of some common bone diseases like osteoporosis [23], where graft resorption and replacement by native bone tissue may not be the best option.

In recent years, the development of 3D printing techniques for the manufacture of ceramic-based scaffold materials has shown promising outcomes [1, 2].

Bioprinting technologies have grown rapidly in the last decade, being also known as “additive manufacturing” or “extrusion bioprinting.” Bioprinting can be defined as a spatial method of stratified deposition of a biological material (or support for biological material), based on a computerized, layer-by-layer model, using a CAD-CAM system.

The structure of the computerized model can be modified and rearranged with the passage of each layer, so as to obtain a complex final model that mimics the tissue structure. The versatility of the technology allows the adoption of an unlimited number of material combinations for extrusion, thus ensuring the possibility of developing unique three-dimensional models, adapted from case to case. Extrusion bioprinting technology is a combination of an automated robotic system, controlled by software and an extrusion distribution system of the material in the custom 3D structure. This process ensures speed but also structural integrity due to the computerized continuous deposition system. 3D models can be obtained, generated, imported, and exported from any CAD system, including data obtained from medical imaging systems such as computer tomography (CT) and/or nuclear magnetic resonance (NMR). The material deposition system can be operated by means of a screw mechanism and stepper motor, pneumatically, by piston-compressed air mechanism, or by solenoid-electromagnetic system. Deposition systems by screw mechanism are more precise, can be better controlled, and also provide controlled deposition in the case of very viscous substances. These deposition systems can be assembled on a 3D bioprinting machine so that they work in synergy, especially if two different materials are deposited. Unlike other additive manufacturing processes, extrusion bioprinting does not require large amounts of energy and is an environmentally friendly method. In addition it has a high standardization capacity and does not require special auxiliary installations. A characteristic is that it can produce, under specific conditions, materials with a porous structure and shape similar to the anatomical one, likely to attain biocompatibility status.

The 3D printing technique allows the manufacturing of scaffold-type materials with complex internal structures and high resolution, designed according to the specific needs of each patient. The technology of extruding materials in the form of

pastes, which are passed through a nozzle or hole to obtain fibers arranged as three-dimensional structures of different shapes, is suitable for the manufacture of hard tissue scaffolds in bone tissue engineering.

Scaffolds are of utmost importance in tissue engineering because they provide the necessary support for cell proliferation and differentiation. Also, the scaffold's architecture defines the final form of the new organ. Biocompatibility of scaffolds made by 3D printing, as well as different aspects of their interaction with cells, has been explored in numerous studies by *in vitro* and *in vivo* tests [21].

The extrusion-based additive manufacturing techniques are favorable for printing scaffold structures due to the ability to process a wide range of biomaterials with controlled porosity and to generate interconnected pores, which represent essential requirements for cell growth [22]. The topography of the surface of the biomaterial as well as its architecture on the micro- and nanoscale plays an important role in bone tissue engineering. Cao et al. have shown increased tissue regeneration and decreased inflammatory reactions in the case of aligned fiber scaffolds, compared to scaffolds whose fibers were randomly arranged [24].

Regarding 3D printing of barium titanate (BT) ceramics for medical applications, Schult et al. [25], have shown that BT powder can serve as a material for bone reconstruction, obtained by 3D printing cylindrical parts with 11.7 mm in diameter and 3.51 mm high, out of the three BT-based mixtures. The first mixture, M1, consisted of untreated BT powder, a stable polymer, and a flow additive—AEROSIL R8200. The second mixture, M2, has the same composition as the first, but BT was previously subjected to a heat treatment of calcination, using for this a fraction of the sieved powder of 60–80  $\mu\text{m}$  and a flow additive. The third mixture, M3, also contains calcined BT, but in this case the fractions <125  $\mu\text{m}$  and 125–250  $\mu\text{m}$  were used in a ratio of 1:2, without adding flow additives, because the powder has good fluidity. To bond the material, a soluble polymer granulate with a mean grain size of 50  $\mu\text{m}$  was used in all three mixtures. Solupor-Binder (Voxeljet AG, Germany) is used as a binder fluid. The binder partially dissolves the polymer granulate so that the ceramic particles glue together. The porosity was visible in all samples, being beneficial for cell growth. After sintering, the largest contraction was observed in the case of the M1 sample, of 75.53%, but the other two also recorded relatively high contractions, M2 of 40.55% and M3 of 29.51%. The results reported in their study confirm that porous barium titanate ceramics can be used as a 3D structure for bone tissue engineering and bone formation can be promoted by electrical stimulation [25].

In other study, a binder jetting additive manufacturing technology was used to fabricate robust geometric barium titanate specimens of  $12 \times 12 \times 3 \text{ mm}^3$  by using commercial BT powder [26]. The results presented in their work have shown that 3D printing allows the manufacture of custom, conformal, geometrically complex piezoelectric devices for next-generation industries such as biomedical ones. One example includes the possibility of an energy-harvesting active biomedical implant, the shape of which could be customized for patient-specific geometry corresponding to anatomical features and use (e.g., a bone implant that will eliminate the need for battery replacement and resulting follow-on surgeries).

## **2. Design of multilayered ceramic materials**

Fractures occur in ceramics as a result of crack propagation. The science of design against fractures is based on the pioneering work of A.A. Griffith (1893–1963) who proposed an energy balance approach to predict fracture strengths in materials [27]. Thus, crack growth is associated with the release of

strain energy and absorption of energy to create the two flanking surfaces. In a succinct manner, we may calculate the stress level  $\sigma_f$  when crack propagation occurs using the Griffith equation:

$$\sigma_f = \sqrt{\frac{2E\gamma}{\pi a}}, \quad (1)$$

where E is the Young modulus,  $\gamma$  is the surface energy, and a is the size of the crack or defect. This describes well very brittle materials, which do not exhibit plasticity domains before fracture. A more general description was developed based on the original Griffith equation by Irwin [28] and Orowan [29] as follows:

$$\sigma_f = \sqrt{\frac{E\zeta_c}{\pi a}}, \quad (2)$$

where critical strain release rate parameter,  $\zeta_c$ , was introduced to consider the energy dissipation into material due to a ductile behavior of the material. A more detailed description of the problem is provided by Roylance [30].

The design of fracture-resistant materials by combining viscoelastic polymers with ceramic materials would be either as composites (separate components) or in the form of mixtures. A composite beam made of multiple layers of ceramics interrupted by polymer layers would be protected against catastrophic crack propagation across layers. Based on the Griffith energy balance approach, it is possible to find out the ceramic layer thickness that would maximize fracture resistance. Griffith equation was historically used to describe fracture resistance dependency on grain size ( $d_{grain}$ ) in carbon steel and thus explain some catastrophic failures of low-grade steels at temperature transitions. At plastic to brittle transition of the material, the crack was considered to propagate along the whole grain and dissipate at grain boundaries. Replacing  $a = d_{grain}$  in Eq. (2), it results:

$$\sigma_f = \sqrt{\frac{E\zeta_c}{\pi d_{grain}}}, \quad (3)$$

Analogously, for a multilayered ceramic material (**Figure 1**) shaped as a beam with equally thick longitudinal layers, we plot fracture stress against layer thickness, considering the most unfavorable situation when the crack expands immediately across the whole layer. The relative units refer to maximal fracture stress and beam thickness for normalization. From the fracture stress curve, it results, at a first view, that very thin layers would provide the beam with maximal protection against fractures. Another criterion for optimization is provided by efficiency reasoning.

Subjected to tensile stress, the beam would distribute the load on individual layers according to their thickness. A maximal fracture-proof design of a multilayered beam would consider that even a single layer would be able to support the whole beam load, meaning that the tension applied on the layer is lower than the beam fracture tension. Intuitively, a beam consisting of two layers is a minimal backup mechanism, whereas more layers may look excessive for most applications. In the graph in **Figure 1**, the intersection between the two curves occurs for a number of 10 layers. In other words, for a beam designed to resist fracture, more than 10 layers would not provide reliance on single layer last standing (the initial premise), whereas less than this number lowers the fracture-safe tension limit. Therefore 10 longitudinal ceramic layers, uncoupled for fracture propagation, may already provide the safest design for tensile load fractures in a beam. The underlying supposition is that the ultimate tensile strength has the same order of magnitude as the fracture strength. Transversal loads on the beam would require a change in the design of the multilayered beam; still the reasoning example for longitudinal loads demonstrates how to look for the optimal grain size in order to

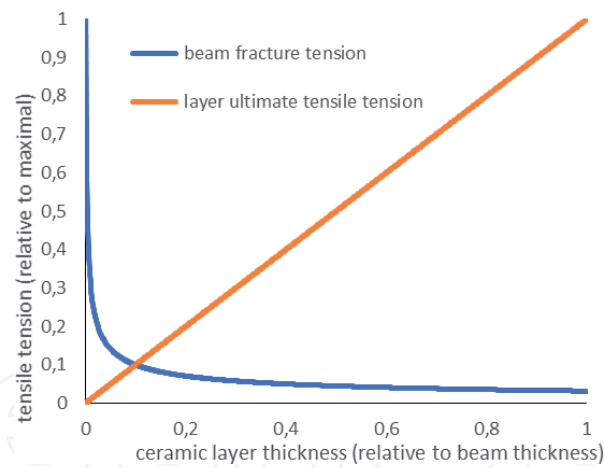


**Figure 1.**

*A proposed criterion for fracture-proof layer thickness in layered beams made of brittle ceramics exposed to longitudinal stretch. Intersection between curves describing ultimate tensile tension of a layer (orange), and beam fracture tension (blue) provides a point of optimal layer thickness to stand alone against the whole beam stretch load.*

build fracture-resistant polymer-reinforced ceramic materials. Thus, decreasing the grain size to nanometer level does not bring additional fracture resistance to millimeter-thick ceramic objects. The 3D printed material in **Figure 5** is made of ceramic-collagen filaments  $\sim 0.6$  mm thick oriented in two perpendicular directions and connected in the nodes. The filaments are made of globular grains 2–10  $\mu\text{m}$  in diameter. This structure actually relies on the binder to hold the grains together. The space between grains is large enough to accommodate biopolymer filaments as binder; one way to produce such filaments in place is to populate the spongy structure with fibroblasts and grow them in culture, as we show here. Then a weak link will reside inside ceramic-polymer hybrid grains.

### 3. Ceramic-polymer hybrid materials

Adding a polymer to a ceramic material in 3D printing is in the first place a mean to modulate the viscosity of the printing paste and support complex 3D structures while they are raised by adding material. Keeping the polymer in place or removing it by post-processing of the printed object depends on the contribution of the polymer to the mechanical properties of the printed object. The brittleness of glasses and ceramic materials is usually addressed by reinforcing the brittle material with elastic fibers, either as composite or as mixture. In mixtures, nanoscale contact between ceramic materials and polymers intimately modulates the elasticity of the resulting material. Aragonite and hydroxyapatite have a very high elastic modulus, around 100 GPa, and a fracture toughness of  $\sim 1 \text{ MPa}/\text{m}^{1/2}$ . With those values, based on some common assumptions, Chen et al. estimated [31] that the brittleness domain of the material is in the nanometer range. Biological structures based on aragonite (nacre) or hydroxyapatite (like bones) rely on elastic biopolymers as binders to increase their fracture resistance by dissipating the stress energy. Irwin and Orowan approach on fracture propagation assumes that stress energy is dissipated around fracture tip by plastic deformations, in which a purely entropic polymer does not accomplish. A mechanism for plastic deformations in nacre resides in micrometer-sized parallel platelets that are able to slide on each other. In this case, the binder breaks and forms attachments to the aragonite platelets while the stress is dissipated. This occurs at a micrometer range. On a nanometer scale, viscoelasticity inside the binding biopolymer may provide another mechanism for stress relaxation.

The idea of mixing collagen and ceramic powder in a paste for printing bone grafts or other bone-like structures for medical applications is based on similarity with the natural bone. Ideally, osseointegration of the grafted material would be accomplished on a long timescale by the progressive action of osteoclasts and osteoblasts which remove the graft material and deposit new bone in place. Having a structure that resembles the natural design may not always respond to functional requirements of a medical application. For example, the porosity of the material should accommodate new osteon growth, requiring 200  $\mu\text{m}$  pore size, to allow growth of new capillaries, optimal for 50  $\mu\text{m}$  pore size, whereas interconnected micropores lower than 10  $\mu\text{m}$  improve the metabolic environment and fluid circulation through capillarity [32]. In a mixture, the viscoelastic polymer should significantly add toughness to effectively dissipate strain energy from initiating cracks in ceramics. A relevant group of biological polymers are the proteins involved in the elasticity of animal tissues. An impressive coordinated effort was made to understand the contribution of the giant protein titin to the elasticity of the striated muscle, detailed on structural, mechanical, and enzymatic description of the functional segments in titin molecules. A comprehensive review on the subject is provided by Prof. Wolfgang A. Linke [33].

The Ig domains in titin were described for their viscoelastic role, protecting titin from breaking under excessive stretch. In 1996, Improta, Politou, and Pastore determined the structure of I27 titin Ig domain by nuclear magnetic resonance (NMR) techniques [34]. The I27 titin Ig domain structure consists in two  $\beta$  sheets packing against each other, each  $\beta$  sheet containing four  $\beta$  strands. Stretch-induced unfolding of the Ig structure provides significant additional extension to the titin molecule, as demonstrated by Linke and Fernandez laboratories [35, 36]. Atomic force microscopy of single molecules was used to investigate synthetic polypeptides based on repetitive Ig domain gene constructs.

In **Figure 2** we replotted from literature some AFM force spectroscopy measurements on collagen I molecules [37], a synthetic polypeptide fragment made of 8 repetitive I27 titin Ig domains [38] and a synthetic protein made of repetitive modules found in dragline spider silk protein (16 SPI and 4 SPII modules) [39]. Extension of collagen molecule in the nanometer range generates almost no force, starting to rise at 300 nm extension. Instead, a single I27 module already provides

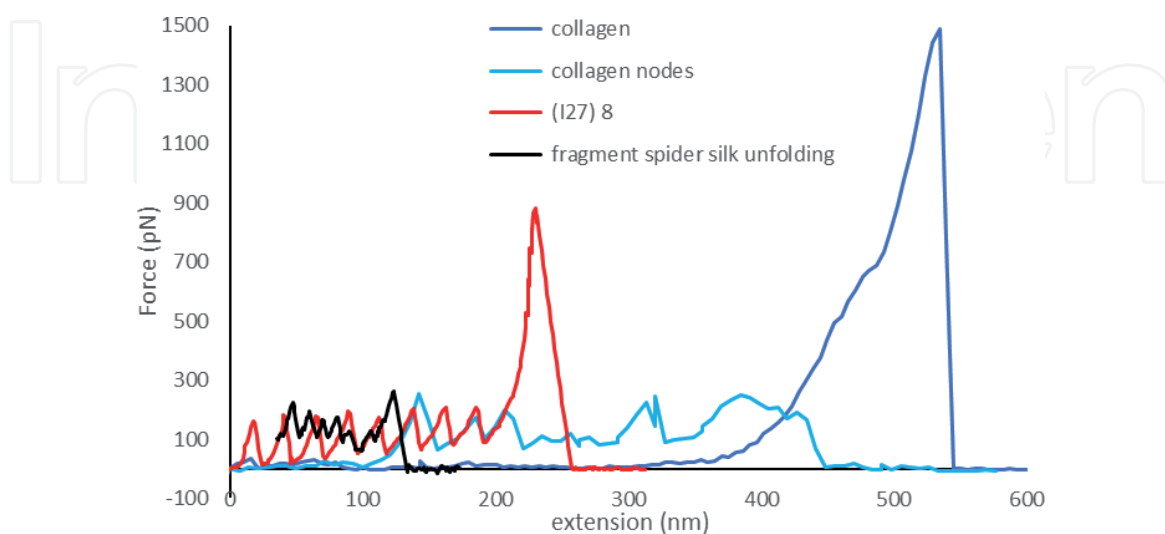


**Figure 2.** Comparison of force extension AFM measurements in collagen I single molecules (blue), collagen I interconnected molecules (light blue), a synthetic polypeptide made of 8 repeats of I27 titin Ig module (red) and a synthetic protein fragment made of repetitive modules from dragline spider silk protein (black). Replotted and adapted from Linke et al. for (I27)<sub>8</sub> [38], Bozec and Horton [37] for collagen I, and Oroudjev et al. [39] for modular recombinant protein from spider silk.

maximal tension of folded state with 28.1 nm stretch and then unfolds and releases a strain (red line). Unfolding and full extension of all 8 I27 repeats in the polypeptide occurs at ~230 nm stretch, raising the force to 882 pN, which is 59% of the maximal single molecule collagen force. Stretching multiple collagen molecules, as they are connected by nodes in a net, also fails to deliver significant force at nanometer range extensions (light blue line). For comparison, a synthetic recombinant modular fragment from dragline spider silk protein is shown to unfold its modules with a repetitive pattern of 14 nm (black line), releasing lower levels of tension than Ig domain unfolding or collagen I molecule node detachment.

Addition of long-range acting binders (developing significant force only at high extensions) versus short-range acting binders in the composition of hybrid polymer-ceramic material is not an obvious decision. Increasing collagen I molecule concentration would raise the number of cross-links between molecules, thus enabling significant force development at lower extensions (as shown in **Figure 2**, light blue line). Ultimately, as concentration is increased, collagen I molecules will assemble in fibrils with high strength and low extensibility ropelike structures, 260–410 nm wide [40]. This will increase the interspacing between mineral grains or tiles to sizes often found in the natural reign of such materials [41]. Mechanical measurements (indentation technique) on collagen fibrils (50–200 nm in diameter) dissected from rat tail showed a Young elastic modulus in the range from 5 GPa to 11.5 GPa (in air, at room temperature) [42], a value at most 1/10 of hydroxyapatite modulus. The concept is that collagen fibers contribute less to the elastic stiffness of the bone and more to its capacity to absorb deformation energy before it fails, that is, toughness [41]. As part of the energy dissipation of the deformative load, the bone structure suffers plastic deformations at the microstructural level, and, in living organisms, it is repaired and even remodeled to withstand the new actual load configuration. If we consider that natural structures evolved to optimize functionality, then it is important to understand that optimization also means maximal toughness or the solution had to deal with limitations and constraints of the cellular machineries that build bone-like biopolymer-mineral structures.

#### 4. 3D printing of ceramic-polymer hybrid materials

Patient-specific design of orthopedic prosthetic devices may improve the durability and the performance of the device by adequate distribution of loads and by using wear-resistant materials on highly solicited spots. An example is hip arthroplasty where bearings may be adequately designed and fabricated to minimize surface friction between elements [43]. With the use of numerical models, the shape and mechanical properties of the prosthesis could be optimized according to patient characteristics like height, weight, gender, and age. Then, the prosthesis has to be engineered for a suitable mounting procedure during the orthopedic intervention and manufactured according to specifications. Some design features like 3D shape may be attained with standard manufacturing techniques, and other features, particularly those involving material microstructure, are possible only by advanced manufacturing. 3D printing combines the advantage of using directly the results of numerical modeling to create the prosthetic device—eliminating some intermediate steps, with the micrometer precision and versatility of the printing mechanism and allowing for microstructuring and the use of various materials for the same piece.

An example of ceramic-polymer hybrid material fabricated by 3D printing method is presented. *For the first time*, 3D hybrid organic-inorganic materials based on barium titanate and collagen (BTC) and barium strontium titanate and collagen (BST-C), with potential applications as filler in bone tissue engineering, have been

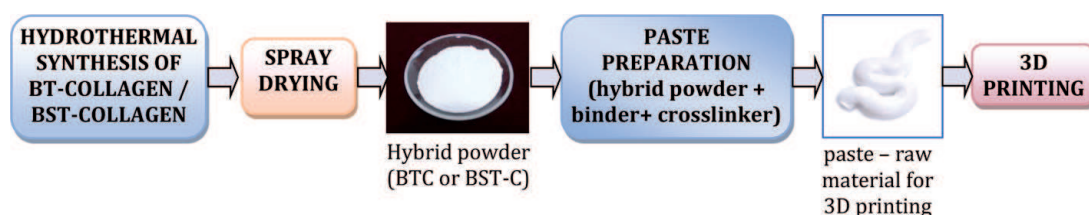


**Figure 3.**  
Technological flow for the fabrication of 3D structures.

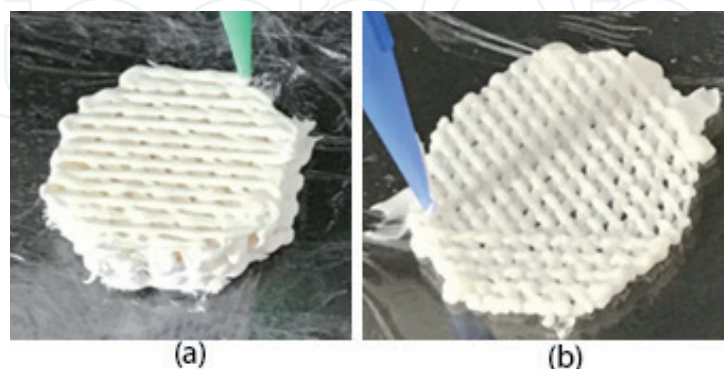


**Figure 4.**  
3D printed scaffolds using two types of nozzles: (a)  $\varnothing$  0.8 mm (BST-C structure) and (b)  $\varnothing$  0.4 mm (BTC structure).

developed by extrusion-based 3D printing method, as presented below. Thus, hybrid nanostructured powders (BTC and BST-C) were obtained by the hydrothermal process at high pressure, starting from  $\text{Ba}(\text{OH})_2 \cdot 8\text{H}_2\text{O}$  powder, aqueous solution of  $\text{TiO}_2\text{Cl}_2$ , and collagen powder as BTC precursors and  $\text{Ba}(\text{OH})_2 \cdot 8\text{H}_2\text{O}$  powder, aqueous solution of  $\text{Sr}(\text{NO}_3)_2$ , aqueous solution of  $\text{TiO}_2\text{Cl}_2$ , and collagen powder as BST-C precursors. After the solution pH was adjusted at  $\text{pH} > 10$ , and the hybrid suspension thus prepared was transferred to the Berghof autoclave (Germany) and subjected to hydrothermal synthesis at  $T < 100^\circ\text{C}$  and  $p = 40$  bar for 2 h. Afterwards, the hybrid nanostructured powders were filtered and washed with distilled water until neutral pH was reached and further spray-dried using a LabPLANT SD-06 spray dryer (UK).

Powders resulted after hydrothermal synthesis were mechanically mixed with a water-soluble polymer binder (Mowiflex, Kuraray Poval) 20% solution and a cross-linking agent (Baymedix<sup>®</sup> FD103, Covestro), obtaining a viscous paste which is further used as a feedstock in the 3D printing process using 3D BioScaffolder system (SYS-ENG, Germany) equipped with BioScaffolder software (SW) 3.0. The technological flow is briefly depicted in **Figure 3** (synthesis of hybrid powders, preparation of paste, and 3D printing of hybrid structures).

Some examples of 3D hybrid structures obtained with different nozzles and rotation angles between 2 successive layers ( $90^\circ$  and  $45^\circ$ , respectively) are given in **Figure 4**.

## 5. Manufacture of 3D structures based on barium titanate and collagen and barium strontium titanate and collagen by 3D printing method

3D printing is a highly versatile technique to fabricate complex structures with high precision and nanometer resolution. The principle of this technique is based on the extrusion of continuous filaments (inks) in a layer-by-layer sequence using

computer-aided design (CAD) tools. This method is capable of fabricating structures with feature sizes on the microscale (0.1–100  $\mu\text{m}$ ) and mesoscale (>100  $\mu\text{m}$ ), depending on the nozzle diameter. The ability to fabricate a variety of structures requires a good control over the formulation and rheological behavior of the inks and the printing parameters (velocity printing, pressure extrusion). The fundamental advantage for any lattice structure are that it is self-supporting (to bear on itself) without the need for inside supports. Another key aspect for the use of porous structures is pore interconnectivity. Porosity is defined as the total percentage of bare spaces in a solid and is a morphological property independent of the material.

The 3D structures were obtained as described above, using the 3D printing technique and BioScaffolder (SYS-ENG, Germany) device, connected via a USB port to a computer on which the BioScaffolder SW 3.0 software is installed. This software allows the configuration of the 3D object to be created in this program or imported from a CAD-CAM program, as well as the setting of the printing process parameters for the 3D object (scaffold), made by depositing several layers of extruded fibers. The shape of 3D structure can be also set using BioScaffolder software. Thus, cubic, octagonal, and cylindric shapes can be obtained.

## 6. Morpho-structural characterization of 3D structures

BTC and BST-C structures fabricated as described above have been characterized using different techniques: scanning electron microscopy coupled with energy dispersive X-ray analysis (SEM/EDX), X-ray diffraction (XRD), and optical profilometry.

SEM/EDX analysis was performed using a FEI E-SEM Quanta 200 microscope equipped with EDX. XRD analysis was performed using a Rigaku MiniFlex 2 diffractometer. Optical profilometry measurements were performed using Veeco WYKO NT1100.

### 6.1 SEM/EDX characterization

SEM images of two representative samples (BTCM-1 and BST-C1) are depicted in **Figures 5** and **6**.

**Figure 5b** shows a typical image of a 3D structure with fibers having thickness of 512–587  $\mu\text{m}$ , while the distance between them varies between 762 and 1093  $\mu\text{m}$ . **Figure 5a** clearly shows how the fibers are arranged in multiple layers in the 3D structure. The round-shaped particles of barium titanate-based nanopowders can be observed in **Figure 7c**, as a result of  $\text{BaTiO}_3$  spray-drying.

In the case of BST-C1 sample, the porosity of the structure can be observed in **Figure 6a** (cross section). The fiber thickness varies between 860 and 1064  $\mu\text{m}$ ,

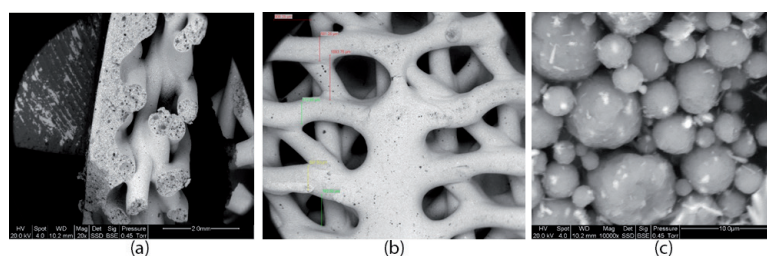


**Figure 5.** SEM images of BTCM sample: (a) cross section of 3D sample; (b) front image at 20 $\times$ ; (c) front image at a higher magnification—10,000 $\times$ .

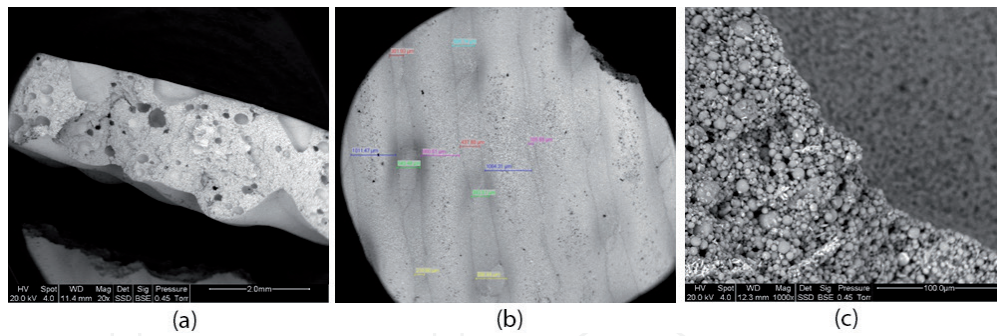


**Figure 6.** SEM images of BST-C1 sample: (a) cross section of 3D sample; (b) front image at 33×; (c) front image at a higher magnification—1000×

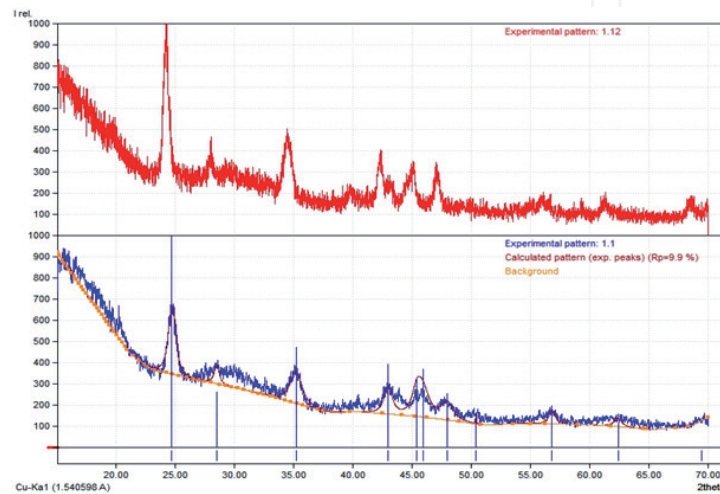


**Figure 7.** XRD spectra of BTCM-1.12 sample (in red) and BST-C1.1 sample (in blue).

Sample	C	O	Ti	Ba	Sr	Total
BTCM-1	9.04	29.59	25.37	36.01	—	100.00
BST-C1	14.22	26.50	10.78	8.42	40.09	100.00

**Table 1.** Semiquantitative analysis of two representative 3D structures (BTCM and BST-C).

while the distance between them is about 105–543 μm (**Figure 6b**). Similar with BTCM-1 sample, spherical particles of  $\text{Ba}_x\text{Sr}_{1-x}\text{TiO}_3$  nanopowders are observed in **Figure 6c**. EDX analysis is presented in **Table 1**.

## 6.2 XRD characterization

XRD spectra of two representative samples (BTCM-1 and BST-C1) are presented in **Figure 7**. From **Figure 7**, it can be seen that the main characteristic peak of  $\text{BaTiO}_3$  in sample BTCM-1 corresponds to  $2\theta = 39.71$  and interplanar distance  $d = 2.268$ . The crystallite size related to this peak is 14.1 nm, and it was calculated using Scherrer equation. In the case of BST-C1 sample, the main characteristic peak appears at  $2\theta = 35.18$  and interplanar distance  $d = 2.549$ . The crystallite size calculated for this peak using Scherrer equation is 8.9 nm. As it can be seen on the diffraction spectra, non-doped barium titanate (BTCM-1) and Sr-doped barium titanate (BST-C1) powders are slightly shifted. Peak locations are not exactly

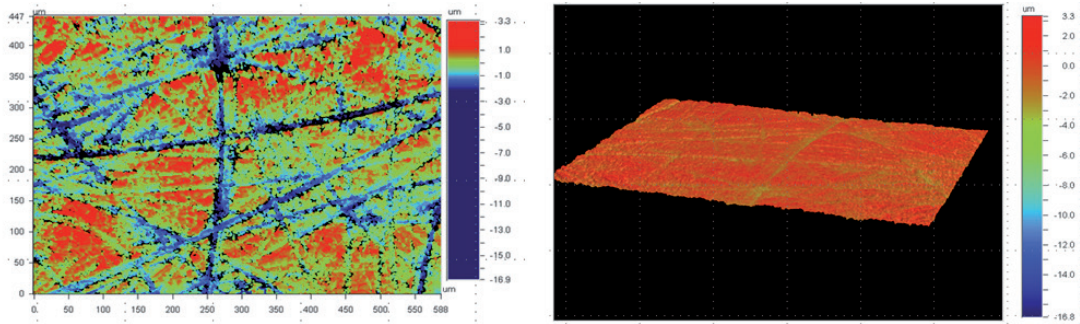


**Figure 8.**  
Surface roughness of BTCM-1.5 sample.

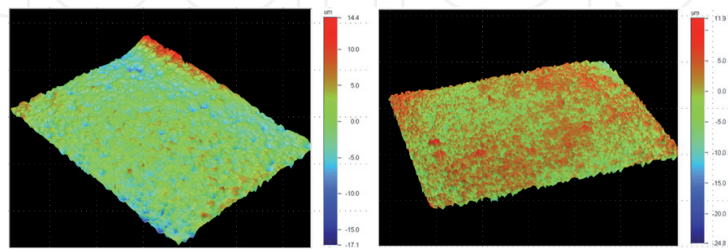


**Figure 9.**  
Surface roughness of BST-C1.3 sample.

suitable to PDF cards of  $\text{BaTiO}_3$  and  $\text{Ba}_x\text{Sr}_{1-x}\text{TiO}_3$ , which might be explained by the presence of binder and collagen in the powder compositions.

### 6.3 Optical profilometry

Surface roughness of two representative samples (BTCM-1.5 and BST-C1.3) is depicted in **Figures 8** and **9**. The mean surface roughness  $R_a$  (the average roughness of the surface) of BTCM-1.5 is about 600 nm.

The mean surface roughness  $R_a$  (the average roughness of the surface) of BST-C1.3 is about 2.29  $\mu\text{m}$ .

## 7. The stability and biocompatibility of BTCM 3D printed materials for in vitro tests

The BTCM materials were sterilized by immersion for 4 h in an 8 ml sterile phosphate buffer containing 1% penicillin/streptomycin and 0.25 mg/ml amphotericin B (Fungizone) and then washed three times with an 8 ml of sterile phosphate buffer to remove the excess of Fungizone and penicillin/streptomycin. After 4 h of sterilization, the BTCM material retains its structure almost intact and can be handled with care in the next steps. The residues released from BTCM materials at the end of the sterilization period were undetectable visually and demonstrated the biomaterial stability in phosphate buffer. After sterilization the materials to be analyzed were moved into an 8 ml completely sterile DMEM culture medium and kept for 24 h in the incubator at 37°C. This step intended to analyze the impact of the soluble compounds released by the materials, if any, in the cell culture medium on cell morphology and adhesion. The DMEM medium resulted from the 24 h of incubation with BTCM materials was further used for culturing 1070Sk CCD fibroblasts and SKMel23 metastatic melanoma cells. The CCD fibroblasts (passage 23) and SKMel23 melanoma cells (passage 3) were seeded in a cell culture six-well plate at a density of  $2 \times 10^4$  cells/well, cultured in DMEM medium

(control) or DMEM medium resulted from incubation with BTCM materials, for 24 h, and analyzed in bright-field microscopy. The fibroblasts grown in the DMEM medium exposed to the BTCM material were completely adhered to the substrate and had a morphology similar to the controls (**Figure 10**). In the case of SkMel23 cells grown in DMEM exposed to BTCM material, the cells also well adhered to the substrate. However, their morphology was slightly different compared to the control cells (**Figure 11**). Next we investigated whether SkMel23 cells were able to adhere to the BTCM material itself. For this purpose, a suspension

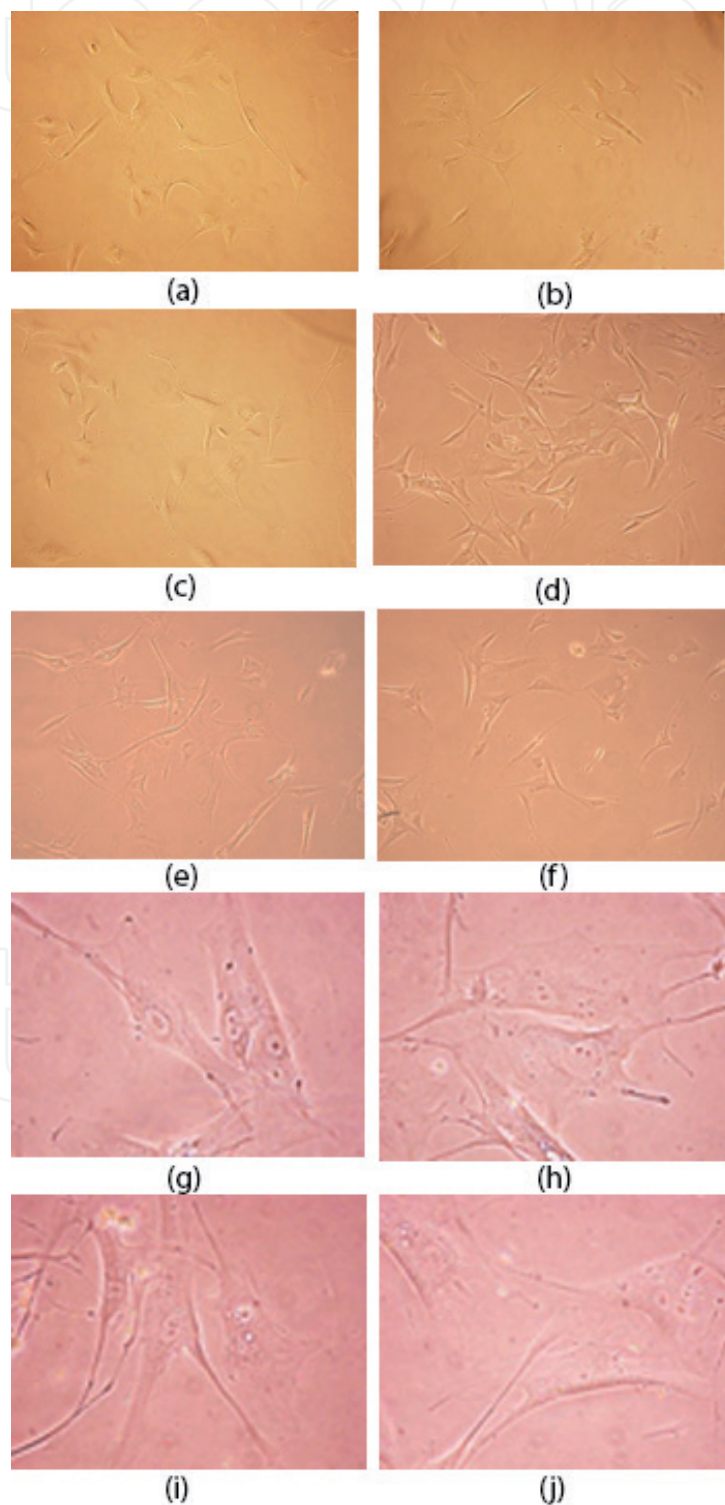


**Figure 10.** Fibroblasts grown in DMEM (a, b, c, g, h) compared to fibroblasts grown in DMEM previously exposed to BTCM material for 24 h (d, e, f, i, j) (bright-field microscopy, 10× magnification, a–f, and 40× magnification, g–j).

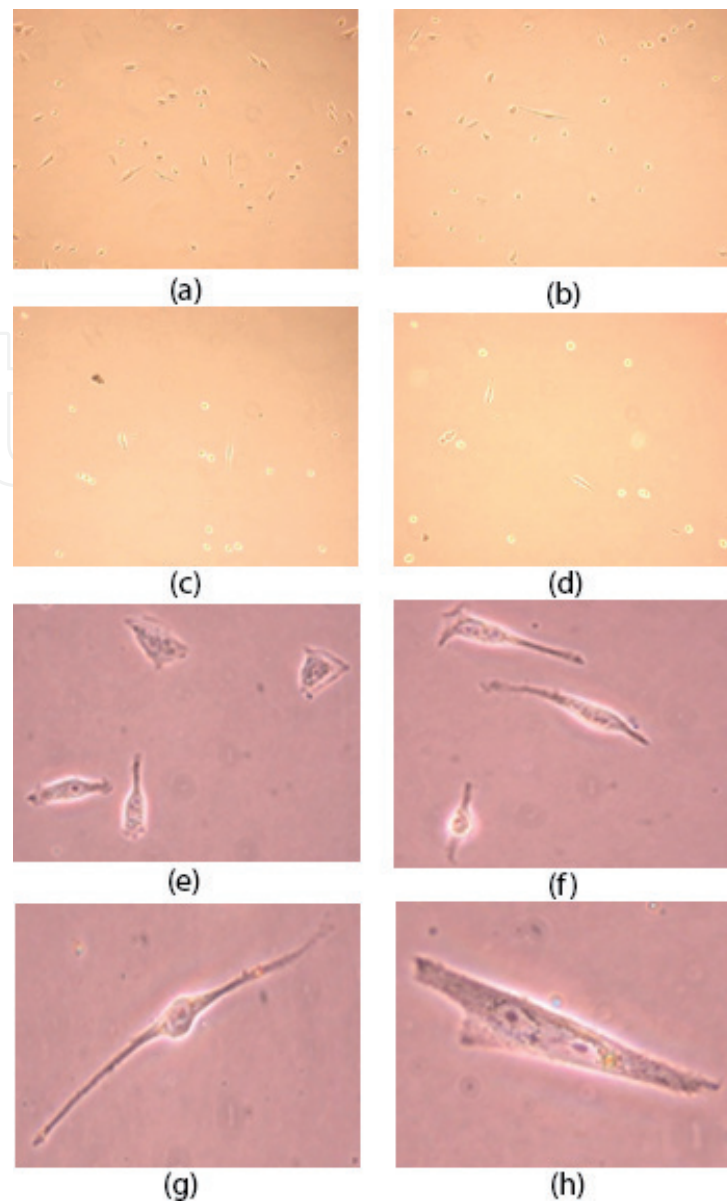


**Figure 11.**

*SkMel23 cells grown in DMEM (a, b, e, f) compared to SKMel23 cells grown in DMEM previously exposed to BTCM material for 24 h (c, d, g, h) (bright-field microscopy 10× magnification, a–d and 40× magnification, e–h).*

containing  $100 \times 10^4$  SKMel23 cells in an 8 ml complete DMEM medium was added onto the sterilized BTCM material and previously preincubated in DMEM according to the protocol described above and further cultured for 24 h in complete DMEM medium.

After 24 h the culture medium was removed, and the BTCM material was washed three times with 8 ml of sterile PBS. The material was then moved using a sterile metal spatula to another six-well plate in order to evaluate only the cells adhered to the material and to exclude those that adhered to the plastic surface of the well. The BTCM material was incubated with 8 ml of sterile trypsin for 10 min, at 37°C with gentle shaking every 3 min to ensure a good detachment of cells. The supernatant was transferred to a 15 ml tube to which 6 ml of complete DMEM was added for trypsin neutralization and was centrifuged for 5 min, at 1500 rpm. The cell pellet was recovered at the bottom of the tube, and cells were counted after dilution 1/1 with trypan blue, which stains only the dead cells. From  $100 \times 10^4$  SkMel23 cells seeded on BTCM material, a number of  $8 \times 10^4$  cells were recovered after 24 h, which indicates that at least 8% of SkMel23 cells were able to adhere to BTCM material.

## 8. Conclusions

Materials based on BT or BST and collagen are candidates for medical applications in bone reconstruction and enhancement, suitable for 3D printing technologies that allow patient-specific shape, microstructure, and composition of the artificial bone. Artificial graft osteointegration at the interface with the natural bone will be facilitated by a printed porous structure that allows cellular infiltration, adherence, and growth. An example of ceramic-polymer hybrid material fabricated by 3D printing method was presented here. *For the first time*, 3D hybrid organic-inorganic materials based on barium titanate and collagen (BTC) and barium strontium titanate and collagen (BST-C), with potential applications as filler in bone tissue engineering, have been developed by integrating hydrothermal synthesis with additive manufacturing (extrusion-based 3D printing method). Morpho-structural characterization of 3D structures clearly showed multiple layers of fibers deposited at various angles in the 3D structure. Fiber thickness is around 500–600  $\mu\text{m}$  in the case of BTCM sample. Both BTCM and BST-C samples are composed of spherical particles with crystallite size (estimated from X-ray diffraction patterns) of 14.1 nm (for BTCM) and 8.9 nm (for BST-C).

The 3D printed BTCM materials are physically stable and do not release toxic soluble compounds in cell culture medium. The BTCM material structure allows the adhesion of SkMel23 cells and possibly of other cell phenotypes as well. The cells recovered after being in contact with 3D printed BTCM materials are fully viable.

Mechanical properties of the 3D printed bone graft may be modulated at the nanometer scale by addition of collagen or other biopolymers into the printing paste, whereas at the microscale a composite structure could be completed by the infiltrating cells lying down on the collagen fibers. We propose some criteria to design bone materials that may share the remarkable toughness and self-repairing capabilities of the natural bone and the improved fracture resistance conferred by novel biopolymer-ceramic hybrid printing pastes. The 3D printing technology is thus suitable to address various bone pathologies, ranging from traumatic bone destruction to anomalous remodeling that occurs in osteoporosis. The results we presented here recommend the novel 3D structures as potentially biocompatible and support their use for further in vitro or animal model assays.

## Acknowledgements

Financial support of National Core Programme project no. PN 18070101/2018 is gratefully acknowledged. The authors thank Eng. Raluca Elena Irimescu (IMNR) for the experimental work performed during STSM stage at Technion–Israel Institute of Technology in the frame of COST Action CA 15102, CRM-EXTREME. The authors also thank Ludmila Levin (Technion) for performing the SEM/EDX analysis and XRD analysis and Dudi Badler (Technion) for performing the optical profilometry measurement.

## Conflict of interest

The authors declare no conflict of interest.

IntechOpen

## Author details

Roxana Mioara Piticescu<sup>1</sup>, Laura Madalina Cursaru<sup>1\*</sup>, Gabriela Negroiu<sup>2</sup>,  
Cristina Florentina Ciobota<sup>1</sup>, Ciprian Neagoie<sup>1</sup> and Daniel Safranchik<sup>3</sup>

1 National R&D Institute for Non-Ferrous and Rare Metals—IMNR, Pantelimon,  
Romania

2 Institute of Biochemistry of the Romanian Academy—IBAR, Bucharest, Romania

3 Technion Research and Development Foundation, The Israel Institute of Metals,  
Technion Israel Institute of Technology, Haifa, Israel

\*Address all correspondence to: mpopescu@imnr.ro

## IntechOpen

© 2020 The Author(s). Licensee IntechOpen. This chapter is distributed under the terms of the Creative Commons Attribution License (<http://creativecommons.org/licenses/by/3.0>), which permits unrestricted use, distribution, and reproduction in any medium, provided the original work is properly cited. 

## References

- [1] Jazayeri HE, Rodriguez-Romero M, Razavi M, Tahriri M, Ganjawalla K, Rasoulianboroujeni M, et al. The cross-disciplinary emergence of 3D printed bioceramic scaffolds in orthopedic bioengineering. *Ceramics International*. 2018;**44**:1-9
- [2] Tariverdian T, Behnamghader A, Milan PB, Barzegar-Bafrooei H, Mozafari M. 3D-printed barium strontium titanate-based piezoelectric scaffolds for bone tissue engineering. *Ceramics International*. 2019;**45**:14029-14038
- [3] Jiao H, Zhao K, Bian T, Tang Y. Hydrothermal synthesis and properties characterization of barium titanate/hydroxyapatite spherical nanocomposite materials. *Journal of Alloys and Compounds*. 2017;**715**:73-82
- [4] Ehterami A, Kazemi M, Nazari B, Saraeian P, Azami M. Fabrication and characterization of highly porous barium titanate based scaffold coated by Gel/HA nanocomposite with high piezoelectric coefficient for bone tissue engineering applications. *Journal of the Mechanical Behavior of Biomedical Materials*. 2018;**79**:195-202
- [5] Tang Y, Wu C, Wu Z, Hu L, Zhang W, Zhao K. Fabrication and in vitro biological properties of piezoelectric bioceramics for bone regeneration. *Scientific Reports*. 2017;**43360**:1-12
- [6] Anderson JC, Eriksson C. Piezoelectric properties of dry and wet bone. *Nature*. 1970;**227**:491-492
- [7] Yasuda I. On the piezoelectric activity of bone. *Journal of the Japanese Orthopedic Surgery Society*. 1954;**28**:267
- [8] Fukada E, Yasuda I. On the piezoelectric effect of bone. *Journal of the Physical Society of Japan*. 1957;**12**:1158-1162
- [9] Bassett CA, Becker RO. Generation of electric potentials by bone in response to mechanical stress. *Science*. 1962;**28**:1063-1064
- [10] Nakamura M, Hiratai R, Yamashita K. Bone mineral as an electrical energy reservoir. *Journal of Biomedical Materials Research. Part A*. 2012;**100**:1368-1374
- [11] Bassett CA, Pawluk RJ, Becker RO. Effects of electric currents on bone in vivo. *Nature*. 1964;**204**:652-654
- [12] McElhaney JH. The charge distribution on the human femur due to load. *Journal of Bone and Joint Surgery. American Volume*. 1967;**49**:1561-1571
- [13] Park JB, Lake RS. *Biomaterials: An Introduction*. 2nd ed. New York: Plenum Press; 1992
- [14] Wolff J *The Law of Bone Remodelling*. Berlin: Springer Verlag; 1986
- [15] Zhang Y, Chen L, Zeng J, Zhou K, Zhang D. Aligned porous barium titanate/hydroxyapatite composites with high piezoelectric coefficients for bone tissue engineering. *Materials Science and Engineering C*. 2014;**39**:143-149
- [16] Ribeiro C, Sencadas V, Correia DM, Lanceros-Méndez S. Piezoelectric polymers as biomaterials for tissue engineering applications. *Colloid Surface B*. 2015;**136**:46-55
- [17] Rajabi AH, Jaffe M, Arinzeh TL. Piezoelectric materials for tissue regeneration: A review. *Acta Biomaterialia*. 2015;**24**:12-23
- [18] Feng JQ, Yuan HP, Zhang XD. Promotion of osteogenesis by a

piezoelectric biological ceramic. *Biomaterials*. 1997;**18**:1531-1534

[19] Jones JR, Ehrenfried LM, Hench LL. Optimising bioactive glass scaffolds for bone tissue engineering. *Biomaterials*. 2006;**27**:964-973

[20] Khosla S, Westendorf JJ, Oursler MJ. Building bone to reverse osteoporosis and repair fractures. *The Journal of Clinical Investigation*. 2008;**118**:421-428

[21] Senatov FS, Niaza KV, Stepashkin AA, Kaloshkin SD. Low-cycle fatigue behavior of 3D-printed PLA-based porous scaffolds. *Composites Part B: Engineering*. 2016;**97**:193-200

[22] Zhong G, Vaezi M, Liu P, Pan L, Yang S. Characterization approach on the extrusion process of bioceramics for the 3D printing of bone tissue engineering scaffolds. *Ceramics International*. 2017;**43**:13860-13868

[23] Kim S, Ahn T, Han MH, Bae C, Oh DS. Wicking property of graft material enhanced bone regeneration in the ovariectomized rat model. *Tissue Engineering and Regenerative Medicine*. 2018;**15**(4):503-510

[24] Turnbull G, Clarke J, Picard F, Riches P, Jia L, Han F, et al. 3D bioactive composite scaffolds for bone tissue engineering. *Bioactive Materials*. 2018;**3**:278-314

[25] Schult M, Buckow E, Seitz H. Experimental studies on 3D printing of barium titanate ceramics for medical applications. *Current Directions in Biomedical Engineering*. 2016;**2**(1):95-99

[26] Gaytan SM, Cadena MA, Karim H, Delfin D, Lin Y, Espalin D, et al. Fabrication of barium titanate by binder jetting additive manufacturing technology. *Ceramics International*. 2015;**41**:6610-6619

[27] Griffith AA. The phenomena of rupture and flow in solids. *Philosophical Transactions, Series A*. 1921;**221**:163-198

[28] Irwin GR. Fracture dynamics. In: *Fracturing of Metals*. Cleveland, OH: American Society for Metals; 1948. pp. 147-166

[29] Orowan E. Fracture and strength of solids. *Reports on Progress in Physics*. 1949;**12**:185-232

[30] Roylance D. Introduction to fracture mechanics. In: *3.11 Mechanics of Materials*. Massachusetts Institute of Technology: MIT OpenCourseWare; 2001. Available from: <http://ocw.mit.edu/>

[31] Chen PY, Lin AY, Lin YS, Seki Y, Stokes AG, Peyras J, et al. Structure and mechanical properties of selected biological materials. *Journal of the Mechanical Behavior of Biomedical Materials*. 2008;**1**:208-226

[32] Diaz-Rodriguez P, López-Álvarez M, Serra J, González P, Landín M. Current stage of marine ceramic grafts for 3D bone tissue regeneration. *Marine Drugs*. 2019;**17**(8):471. DOI: 10.3390/md17080471

[33] Linke WA, Hamdani N. Gigantic business: Titin properties and function through thick and thin. *Circulation Research*. 2014;**114**:1052-1068

[34] Improta S, Politou AS, Pastore A. Immunoglobulin-like modules from titin I-band: Extensible components of muscle elasticity. *Structure*. 1996;**4**:323-337

[35] Li H, Linke WA, Oberhauser AF, Carrion-Vazquez M, Kerkvliet JG, Lu H, et al. Reverse engineering of the giant muscle protein titin. *Nature*. 2002;**418**:998-1002

[36] Minajeva A, Kulke M, Fernandez JM, Linke WA. Unfolding of

titin domains explains the viscoelastic behavior of skeletal myofibrils. *Biophysical Journal*. 2001;**80**:1442-1451

[37] Bozec L, Horton M. Topography and mechanical properties of single molecules of type I collagen using atomic force microscopy. *Biophysical Journal*. 2005;**88**:4223-4231

[38] Linke WA, Kulke M, Li H, Fujita-Becker S, Neagoe C, Manstein DJ, et al. PEVK domain of titin: An entropic spring with actin-binding properties. *Journal of Structural Biology*. 2002;**137**:194-205

[39] Oroudjev E, Soares J, Arcdiacono S, Thompson JB, Fossey SA, Hansma HG. Segmented nanofibers of spider dragline silk: Atomic force microscopy and single-molecule force spectroscopy. *Proceedings of the National Academy of Sciences of the United States of America*. 2002;**99**:6460-6465

[40] Bozec L, van der Heijden G, Horton M. Collagen fibrils: Nanoscale ropes. *Biophysical Journal*. 2007;**92**:70-75

[41] Meyers MA, McKittrick J, Chen PY. Structural biological materials: Critical mechanics-materials connections. *Science*. 2013;**339**:773-779

[42] Wenger MPE, Bozec L, Horton M, Mesquida P. Mechanical properties of collagen fibrils. *Biophysical Journal*. 2007;**93**:1255-1263

[43] Piriou P, Ouenzerfi G, Migaud H, Renault E, Massi F, Serrault M. A numerical model to reproduce squeaking of ceramic-on-ceramic total hip arthroplasty. Influence of design and material. *Orthopaedics & Traumatology, Surgery & Research*. 2016;**102**:S229-S234